THE JOURNAL OF PHYSICAL CHEMISTRY B

Article

pubs.acs.org/JPCB

Non-Boltzmann Population Distributions during Single-Bubble Sonoluminescence

David J. Flannigan*,† and Kenneth S. Suslick*,‡

†Department of Chemical Engineering and Materials Science, University of Minnesota, 421 Washington Avenue SE, Minneapolis, Minnesota 55455, United States

‡Department of Chemistry, University of Illinois at Urbana−Champaign, 600 South Mathews Avenue, Urbana, Illinois 61801, United States

ABSTRACT: Single-bubble sonoluminescence (SBSL) spectra from aqueous sulfuric acid solutions containing dissolved neon show widely varying emission despite being similar in chemical composition. From a 65 wt % solution, emission from hydroxyl radicals is observed, with the rovibronic progression being well-described by a single temperature of 7600 K. From an 80 wt % solution, however, emission spectra reveal vibrationally hot sulfur monoxide (SO; T_v = 2400 K) that is also rotationally cold (T_r = 280 K). Further, the SO vibrational population distribution is best-described by a non-Boltzmann distribution. Excited neon atom emission observed from the 80 wt % solution gives an estimated temperature of only 3400 K, indicative of emission from a cool outer shell at the interfacial region. The neon atom excited-state population is also best-described by a non-Boltzmann distribution. These observations are consistent with SBSL emission having both a spatial and temporal component, and the implications for these effects are discussed.

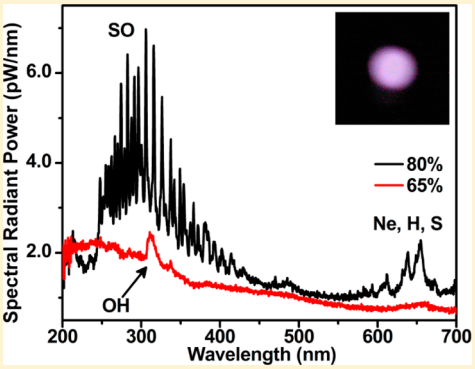

INTRODUCTION

The energetic implosion of a single acoustically levitated bubble driven into repeatable nonlinear oscillations can generate brief but extreme conditions in an otherwise cool liquid. A signature of these extreme conditions is the emission of a flash of light during the maximum implosion of the bubble, a phenomenon known as single-bubble sonoluminescence (SBSL).[1−4] Typically, SBSL spectra are broadband, ranging from the UV to the near-IR.[5] Recent expansion of the liquid parameter space to include concentrated aqueous solutions of mineral acids (e.g., H_2SO_4 and H_3PO_4) has resulted in a wealth of quantifiable information about the intracavity conditions generated during SBSL. Indeed, the spectra observed from such solutions are rich with lines from molecules, atoms, and ions, the properties of which provide a means to quantify temperatures, pressures, and plasma conditions.[6−9] Concentrated solutions of mineral acids are ideal for SBSL studies due, at least in part, to their modest vapor pressures and, thus, the low number density of molecular species inside the bubble compared to more volatile liquids (e.g., water). This translates into more compressional energy per atom/molecule inside the bubble and more intense light emission due to an overall reduction in non-radiative endothermic channels.[10−12]

Previously, we reported that SBSL from degassed 85 wt % H_2SO_4 containing a small amount of dissolved neon showed emission from both atomic (neon) and molecular (sulfur monoxide, SO) species.[7,8] Neon emission occurs from the 3p−3s manifold, with the 3p states being over 18 eV in energy. The emission bands from SO are mainly due to transitions between the $\nu' = 0$ to 3 vibrational levels in the $B\ ^3\Sigma^-$ excited state and levels of the $X\ ^3\Sigma^-$ ground state. At elevated acoustic driving pressures, population of vibrational levels of the SO $A\ ^3\Pi$ state is observed, as is also found during energetic electron impact with SO_2.[13] Population of different levels in the B state allowed for the determination of relatively modest SO vibrational temperatures of 1500 to 3500 K, depending upon the applied acoustic driving pressure.[7] More recently, our group observed significantly higher vibrational temperatures of nearly 10 000 K during SBSL from 65 wt % H_3PO_4 by simulation of hydroxyl radical (OH) rovibrational emission spectra.[9] These high temperatures are remarkable, especially when one considers that 65 wt % H_3PO_4 has a vapor pressure over 200 times higher than that of the 85 wt % H_2SO_4 solution used in the aforementioned studies. One would have expected the SO emission to show higher temperatures due to a larger number density of polyatomic molecules inside the H_3PO_4 bubble. Note that the bond energy of SO is larger than that of OH (5.43 vs 4.81 eV, respectively), so limitations of the former as a temperature probe due to dissociation do not account for the apparent paradox.

The observations described above appear to be at odds with the picture of vapor pressure as a limiting factor for the conditions generated during cavitation. While there is substantial evidence indicating the conditions are limited by

Special Issue: Michael D. Fayer Festschrift

Received: September 15, 2013
Published: October 7, 2013

the thermochemical properties of the bubble contents,[10−12,14−16] other factors could become dominant at low vapor pressures (e.g., formation of a dense plasma), thus leading to apparent disagreement with current theories. For example, little progress has been made in elucidating specific formation mechanisms of the emitting species,[15] and the nature of the bubble/liquid interfacial region and its role in sonoluminescence processes remains ill-defined.[17−20] Further, data pertaining to when and from where within the bubble specific types of species emit photons is challenging to obtain experimentally. This is mainly due to the small volume of the emitting region (~1 μm^3), the short flash duration (~1 ns), and the optical opacity of the dense plasma formed (~10^{21} cm^{-3}).[21−23] If line emission is observable only from a limited spatiotemporal region or if the molecular and atomic reporters are not uniformly distributed throughout the bubble interior, the conditions determined from the lines will not be representative of the entire emitting volume. This is because emission line intensities and profiles reflect the intracavity conditions in the immediate vicinity of the emitter.[7,22,24] It is precisely this sensitivity to local environment, however, that makes emission line intensities and profiles ideal probes for the development of a spatiotemporally resolved molecular-level picture of the processes at work during SBSL.

Here, we report two findings: (1) the observation of dramatically different emission spectra and molecular rovibrational temperatures from degassed 65 and 80 wt % aqueous H_2SO_4 solutions, both regassed with neon, and (2) evidence for non-thermal rovibrational emission from SO as well as apparent non-thermal emission from atomic neon. For the differing spectral profiles, SBSL from the 65 wt % solution shows strong OH emission in the near-UV and essentially no neon emission, while the 80 wt % solution shows strong SO rovibrational progressions as well as lines from neon, hydrogen, and sulfur atoms. These differences arise despite the vapor-phase compositions of the two solutions being similar in terms of types and relative concentrations of species, though the vapor pressures differ by nearly a factor of 20 (2.24 vs 0.12 Torr at 298 K for 65 and 80 wt %, respectively). Further, the vibrational temperature (T_v) of OH from the 65 wt % solution is 7600 K, while for SO in the 80 wt % solution it is only 2400 K (for a best-fit Boltzmann vibrational population distribution).

Perhaps most striking is evidence of non-thermal emission from both molecules and atoms in the SBSL spectra. From the 80 wt % solution, the SO emission is rotationally cold (T_r = 280 K) and non-equilibrated with the vibrational temperatures. Further, improved fits to the time-averaged experimental spectra are obtained by using non-thermal vibrational population distributions, thus indicating the conditions are not adequately described by a single temperature. This is further reflected in the observed atomic emission lines; several neon lines are poorly matched by an otherwise overall best-fit calculated spectrum thermally equilibrated at 3400 K. These results from the 80 wt % solution stand in stark contrast to those obtained from 65 wt %. For OH (from the 65 wt % solution), the rovibrational temperature is thermally equilibrated at 7600 K, much higher than the temperatures observed from the 80 wt % solution. We propose that, based upon the compositions of the various phases and the observations made, that the spatial locations of the emitting species inside the bubble are different for the different solutions. The difference in T_v and T_r suggests OH emission occurs from the vapor interior, while SO experiences a dynamical constraint to formation within a hot liquid/vapor shell at the interfacial region, thus rendering it rotationally cold. Further, observation of non-Boltzmann population distributions for both SO and neon suggests contribution by a non-equilibrated plasma to the otherwise dominant (equilibrated) emission spectra.

EXPERIMENTAL SECTION

Solution Preparation. We now describe the methods unique to the SBSL experiments reported here. The SBSL resonator, a method for generating and levitating a single sonoluminescing bubble, detection system for acquiring the emission spectra and necessary corrections applied to the spectra are described in detail elsewhere.[6,25] Solutions were prepared by diluting 95 wt % H_2SO_4 [Mallinckrodt, AR Select (ACS), used as received] to the desired concentration with nanopure water (Barnstead NANOpure, 18 MΩ·cm, 0.2 μm filters). After dilution, solutions were completely degassed with a direct-drive vacuum pump (<0.1 Torr) with vigorous stirring for 24 h. After degassing, solutions were equilibrated with an overhead pressure of 50 Torr of neon (Matheson, 99.995%) with vigorous stirring at 25 °C for 1 h. After regassing, the solution was transferred directly to the SBSL resonator.

SO Synthetic Spectra. Synthetic SO rovibronic emission spectra were calculated using PGOPHER.[26] Provided the necessary molecular constants for the states of interest are known, PGOPHER can be programmed by the user to simulate the emission spectra of polyatomic molecules. Here, we used the molecular constants reported by Clerbaux and Colin for the $X\ ^3\Sigma^-$ ground state for ν'' = 0−23,[27] while for the $B\ ^3\Sigma^-$ excited state we used the constants reported by Liu et al. for ν' = 0−3.[28] The Franck−Condon factors reported by Yamasaki et al. were used for all possible transitions involving the B and X states.[29] Details concerning the equations used and steps necessary for simulating the molecular emission spectra can be found in the PGOPHER user's guide. It was necessary to perform a background correction to the SBSL SO experimental spectrum before simulation. The underlying continuum in the wavelength range 300−380 nm was fit using a fourth-degree polynomial. The wavelength range was from 300 to 380 nm to avoid complication due to the $A\ ^3\Pi$ state of SO; the often-used assumption that the transition moment is independent of the internuclear separation does not hold for this state (i.e., the Franck−Condon factors for the A state of SO predict population distributions that are not observed experimentally).[30] Therefore, only emission from transitions from the first four vibrational levels of the $B\ ^3\Sigma^-$ state were considered; SO undergoes a predissociation above ν' = 3 for this state.[28]

The fixed and floated parameters, their values, and one standard deviation for the SO synthetic spectrum having an equilibrated vibrational temperature (T_v = 2400 K) with T_r = 280 K are shown in Table 1. For the non-equilibrated synthetic spectrum, all parameters were the same except the relative populations of vibrational levels were floated to achieve an overall best-fit to the experimental spectrum. As was true for all simulations, the fit range and instrument resolution were fixed. The instrument resolution (0.30 ± 0.04 nm) corresponds to the full width at half-maximum (fwhm) value for the lines from a low-pressure Hg(Ar) pen lamp acquired using the same experimental configuration as was used for the SBSL spectra. All experiments reported here were done at this resolution. The least-squares fitting procedure consisted of initial guesses for the floated parameters. This was followed by repeated contour fitting routines within PGOPHER until the error was

dx.doi.org/10.1021/jp409222x | J. Phys. Chem. B 2013, 117, 15886−15893

Table 1. Parameters and Their Values for the Equilibrated Synthetic SO Emission Spectrum[a]

parameter	value/type	one σ
temperature (T_v)[b] (K)	2413	102
temperature (T_r)[c] (K)	282	12
width of Lorentzian component (nm)	1.013	0.084
line shape[d]	Voigt	N/A
spectrum offset (nm)	−0.385	0.266
spectrum scaling factor (a.u.)	1.005	0.001
baseline scaling factor (a.u.)	0.240	0.015
intensity scaling factor (a.u.)	9981.149	541.568
fit range[d] (nm)	300−380	
instrumental resolution[d] (nm)	0.30	0.04

[a]Units in air. [b]Vibrational temperature. [c]Rotational temperature. [d]Fixed parameter.

minimized. The standard deviations of the parameters were determined from the quality of the fit in PGOPHER.

OH Synthetic Spectra. Simulation of the SBSL OH emission spectrum was performed using LIFBASE v.2.0.64.[31] Details of the equations used and physical processes considered within LIFBASE can be found in the user's guide. It was not necessary to perform a background correction to the SBSL OH experimental spectrum before simulation because the spectral radiant power of the underlying continuum in the simulation range (306−335 nm) does not vary significantly. The parameters and their values for reaching the minimum chi-square are shown in Table 2. The minimum chi-square was

Table 2. Parameters and Their Values for the Minimum Chi-Square Fit of the OH Emission Spectrum[a]

parameter	value/type	one σ
temperature ($T_r = T_v$)[b] (K)	7630	550
pressure[c] (atm)	2590	190
spectrum shift[d] (nm)	0	
baseline correction[d] (a.u.)	0	
line shape[d]	Voigt	N/A
% Lorentzian[d]	90	
fit range[d] (nm)	306−335	
instrumental resolution[d] (nm)	0.30	0.04

[a]χ^2 = 12.2487. Peak correlation = 0.995668. Doppler broadening = 0.004862 nm. Total resolution (instrument + broadening) = 1.31675 nm. Collisional broadening and red-shift = 1.04605 nm. Units in air. [b]Assume fully thermalized. [c]Collisional (dispersion) pressure broadening only; LIFBASE does not consider Stark effects. [d]Fixed parameter.

arrived at by iteration of the values for the temperature and pressure, as the fitting is a nonlinear least-squares process. All other parameters were fixed at the values shown in the table and correspond to the experimental configuration. The line shape chosen for the fit was Voigt, as this is a combination of Gaussian and Lorentzian peak functions, both of which are present in SL spectroscopic experiments. The Lorentzian percent contribution to the total line shape was assumed to be 90%, as this will be the major component due to collisional broadening. Note that fitting of typical SBSL emission lines with both Voigt and pseudo-Voigt peak functions returns a weighting factor of 0.9 (i.e., 90%) for the Lorentzian contribution when this parameter is freely floated. Because the lines are broad (typically >1 nm fwhm) in SL studies due to the high intracavity pressures generated during cavitation, the only significant Gaussian contribution to the line shape and width will be the instrument response.[24,32] Note that no wavelength shift was applied to the simulated OH emission spectrum because the red-shift produced by collisional effects provided a precise peak overlap at the pressure parameter value shown in Table 2. This indicates that: (1) the wavelength calibration of the spectrograph was precisely and accurately done and (2) the pressure value reached in the nonlinear least-squares fit is a physically significant value. Note, however, that LIFBASE does not take Stark effects into account, so the value of the pressure parameter should be considered an upper bound.

The instrument resolution and signal-to-noise of the spectrum did not allow for a precise determination of T_r, so the spectrum was assumed to be completely thermalized (i.e., $T_r = T_v$). Nevertheless, it was found that values of T_r higher than T_v produced slightly better fits, while lower T_r values produced dramatically worse fits, indicating that the OH radicals are rotationally hot with a temperature at least that of T_v (7600 K). A non-thermalized simulation with T_r = 300 K (keeping all other parameters the same as in Table 2) is shown for comparison in the Results and Discussion section (Figure 4). Standard deviations of the temperature and pressure parameters were determined by plotting chi-square (χ^2) vs the parameter for which the error is being determined in the region of a local minimum, while keeping all other parameters fixed after finding the global minimum with $T_r = T_v$. The resulting parabolic curve is then least-squares fit with a second-order polynomial (p). One standard deviation (σ) of the parameter of interest (e.g., T) can then be determined from eq 1.[33]

$$\sigma_T = \sqrt{2\left(\frac{d^2p}{dT^2}\right)^{-1}} \quad (1)$$

Neon/Hydrogen/Sulfur Synthetic Spectrum. Simulation of the SBSL neon/hydrogen/sulfur (Ne/H/S) spectrum was performed by custom-programming in Microsoft Excel. The Excel solver tool was used to expedite the fitting process. All electronic transitions having known spectroscopic constants (i.e., wavelength, energy levels, statistical weights, and Einstein transition probabilities) for Ne, H, and S within the fit range (570−680 nm) were considered. All constants used were those reported in the NIST Atomic Spectra Database v.3.1.5.[34] A total of 46 lines was included in the final simulation (38 for Ne, 2 for H, and 6 for S). We also considered lines for oxygen, as well as S^+, Ne^+, and O^+ in the initial simulations. Inclusion of these species did not produce better fits and thus were not considered in the final simulation. The intensity distribution for each of the 46 lines was calculated using a Voigt approximation (eq 2).

$$I = I_0 + S\left[m_u\frac{2}{\pi}\frac{w}{4(\lambda-\lambda_c)^2+w^2} + (1-m_u)\frac{\sqrt{4\ln 2}}{\sqrt{\pi}w}e^{-(4\ln 2/w^2)(\lambda-\lambda_c)^2}\right] \quad (2)$$

In eq 2, I_0 is a baseline offset, m_u is the fractional weight of the Lorentzian component, λ is the wavelength ranging from 570 to 680 nm, λ_c is the unperturbed theoretical peak center position in air, w is the total line width, and S is the peak amplitude given by the expression shown in eq 3.

$$S = \rho \frac{g_i A_i}{Q\lambda_c} e^{-E_i/kT} \quad (3)$$

In eq 3, ρ is the relative number density of atoms, g_i is the statistical weight of the upper energy level involved in transition i, A_i is the Einstein transition probability, E_i is the energy of the upper level for transition i, k is the Boltzmann constant, T is the temperature, and Q is the temperature-dependent electronic partition function, which is given by eq 4.

$$Q(T) = \sum_{i=0}^{n} g_i e^{-E_i/kT} \quad (4)$$

The temperature-dependent electronic partition functions for Ne, H, and S were calculated using an empirical fifth-order polynomial with coefficients determined by L. De Galan et al. and are valid between 1500 and 7000 K (eq 5).[35]

$$Q(T) = a + b\left(\frac{T}{10^3}\right) + c\left(\frac{T}{10^3}\right)^2 + d\left(\frac{T}{10^3}\right)^3 + e\left(\frac{T}{10^3}\right)^4 + f\left(\frac{T}{10^3}\right)^5 \quad (5)$$

For Ne, $a = 1$ and all other coefficients are zero. For H, $a = 2$ and all other coefficients are zero. For S, $a = 6.3025$, $b = 1.2760$, $c = -0.31216$, $d = 0.042862$, and $e = -0.0021798$. Therefore, only the temperature-dependent partition function for S is considered to vary between 1500 and 7000 K; contribution to $Q(T)$ from energy levels higher than 30 000 cm^{-1} (3.72 eV) is less than 0.001, so Q for Ne and H is approximated to the statistical weight of the ground states of those atoms.

Background subtraction of the SBSL Ne/H/S emission spectrum was necessary due to variation of the spectral radiant power of the underlying continuum in this region and because of the sensitivity of the temperature parameter value to the relative intensities of the lines. The background subtraction was performed by fitting the underlying continuum with a fourth-order polynomial. In this way, the intensity for each line at each wavelength position (λ) between 570 and 680 nm was determined numerically, and the total simulated spectrum is a summation of the intensity values at each wavelength position for all 46 lines. The line width (w), line-shift (λ_c + red-shift in nm), relative atom number density (ρ), and baseline offset (I_0) parameters were floated for each of the three atoms, while the temperature was varied systematically by 10 K until a least-squares fit was reached. The values for the parameters that produced the least-squares fit are shown in Table 3.

Because the absolute number densities for the atoms are not known, the radiating species are assumed to be at uniform temperature. In addition, the large differences in energy levels for the different atoms (e.g., >18 eV for the prominent Ne lines compared to 12 eV for H) cannot be used to derive an error for the temperature. Thus, only differences for the energy levels for Ne atoms were considered for error analysis. This, however, produces a large error due to the very small differences in energy (~0.4 eV for Ne). That is, a plot of χ^2 vs T produces a broad parabolic curve having its minimum at 3350 K. Nevertheless, the precision of the simulation (10^{-6} for the squared residuals) allowed for changes of 10 K to be observed in the least-squares fit. Thus, the best fit over the range 570–680 nm can be assigned to 3350 K.

Table 3. Parameters and Their Values for the Least-Squares Fit of the Ne/H/S Emission Spectrum[a]

parameter	neon	hydrogen	sulfur
temperature[b] (K)	3350	3350	3350
partition function at 3350 K[c]	1	2	8.411
line width (nm)	5.597	7.781	1.987
red-shift (nm)	2.303	2.094	2.356
number density (relative)	3.4×10^9	2.0	4.4×10^{-4}
baseline correction		5.7×10^{-17}	
% Lorentzian[d]		90	
range[d] (nm)		570–680	
instrumental resolution[d] (nm)		0.30 ± 0.04	

[a]Sum of squared residuals = 0.96787. Units in air. [b]Temperatures for the three atoms are assumed equal. [c]Fixed for Ne and H; S directly tied to temperature parameter. [d]Fixed parameter.

RESULTS AND DISCUSSION

The SBSL spectra from aqueous solutions of the mineral acids reflect the chemical composition of the bubble interior. For example, SBSL spectra from H_3PO_4 aqueous solutions show only OH emission due to the vapor being comprised entirely of water.[9] In addition, previous work on H_2SO_4 solutions containing sodium sulfate (Na_2SO_4) showed that emission from sodium atoms was observed only at elevated amplitudes of the acoustic driving pressure due to the injection of liquid droplets into the bubble interior.[36] For the solutions employed here, emission profiles dramatically change with modest changes in H_2SO_4 concentration (Figure 1). Though the spectra are quite different in appearance, the bulk liquid compositions as well as the vapor phases (discussed below) of each of the solutions are similar.[37,38] At the concentrations used here, the bulk solutions consist mainly of ion pairs (e.g., $HSO_4^-{\cdot}H_3O^+$) and hydrates of H_2SO_4, and the mole fraction of water is 0.75 and 0.6 for 65 and 80 wt %, respectively. Thus, if droplet injection were at work, one would expect the spectra to be similar in appearance; previous work on SBSL as well as multibubble SL has shown that noble gas emission is quenched when droplet injection becomes dominant.[36,39] Here, however, strong neon lines are observed in conjunction with SO bands up to the highest acoustic pressures used for the 80 wt %

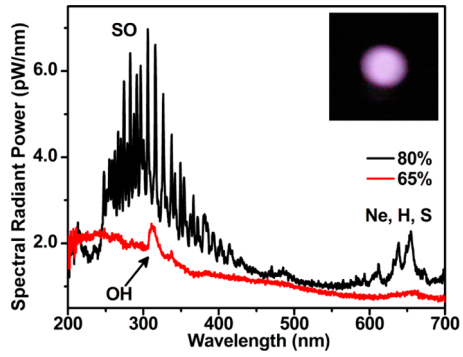

Figure 1. Comparison of SBSL spectral profiles from 65 (red) and 80 (black) wt % H_2SO_4, each regassed with 50 Torr neon. Major features are assigned to the species responsible. The scale for the spectral radiant power applies to both spectra. The inset shows a photograph of a moving single sonoluminescing bubble in the 80 wt % solution. The diameter of the time-averaged sonoluminescing region is 2 mm in diameter. The exposure time was 8 s corresponding to 2.4×10^5 individual SBSL flashes.

dx.doi.org/10.1021/jp409222x | J. Phys. Chem. B 2013, 117, 15886–15893

solution.[7] Therefore, droplet injection as the source of the spectral profiles for either solution is unlikely.

Like the bulk liquid phases, the vapor compositions of the solutions are also very similar. The vapor phase above so-called pure H_2SO_4 is comprised of H_2O, SO_3, and H_2SO_4. This is because H_2SO_4 is actually a component of the more general H_2O-SO_3 binary system. The partial pressures of H_2SO_4 and SO_3 above aqueous sulfuric acid solutions are many orders of magnitude lower than that of H_2O;[38] the vapor composition is essentially comprised entirely of water molecules for both the 65 and 80 wt % solutions. If the vapor phase was the location for the formation and excitation of emitting species, then one would expect to see only OH emission in the spectra from both solutions (as is observed for SBSL from 65 wt % H_3PO_4). That is, while emission from vapor phase species can certainly explain the SBSL spectrum from the 65 wt % solution, it cannot account for that observed from the 80 wt % solution. Therefore, SO must be formed and excited via processes that do not involve either droplet injection or precursor molecules in the vapor interior of the bubble.

The two-site model of sonochemical reactivity indicates that a hot liquid/vapor shell interfacial region, distinct from the interior vapor phase, is a viable site for radical formation and light emission,[18] and this is the most likely location for SO formation and excitation. For the liquid/air interfacial region of H_2SO_4 aqueous solutions, electron and nonlinear optical spectroscopy have been used to show that the overall surface composition matches that of the bulk,[40,41] though the molecular orientations and hydrogen bonding structure differ significantly.[42,43] For 65 wt %, the hydrogen-bonded network structure of water at the interface is similar to that of pure water, while, for 80 wt %, it is significantly less so. Each solution shows far fewer free OH groups (i.e., protruding into the vapor phase) than pure water; 65 wt % has only ~5% that of pure water, while 80 wt % shows none. The formation of ion pairs and hydrates of H_2SO_4 is thought to pull water away from the surface, thus integrating the OH groups into the hydrogen bonding network.[42] Neither solution has free OH groups from H_2SO_4, indicating that the interface is devoid of unbound OH regardless of the parent species. This indicates that the majority of free groups protruding into solution are SO. For both solutions, the free SO groups are from HSO_4^- of the bisulfate/hydronium ion pair, while only the 80 wt % solution has undissociated H_2SO_4 at the interface.[41]

The physical and chemical conditions inside a collapsing bubble at maximum implosion are unlikely to be homogeneous; the conditions in the vapor core should be more extreme than those near the interfacial region where emitting species are in close contact with the bulk liquid heat sink.[18] Thus, the temperatures determined from the observed species will differ if they are emitting from different spatial locations (in addition to possible temporal variation in emission discussed below). Figures 2, 3, and 4 show the relevant sections of the spectra from Figure 1 compared to least-squares fit simulations. The results from Figures 2 and 3 are now discussed; the OH emission spectrum (Figure 4) is discussed below. There are two noteworthy observations to be made from the SO simulations in Figures 2 and 3. The first is that T_r for SO is not equal to T_v (also previously reported in an initial communication of this work).[44] Rather, it is found to be near the bulk liquid temperature. The second is that the observed SO rovibronic emission spectrum is best-fit with a non-Boltzmann vibrational level population distribution (Figure 3).

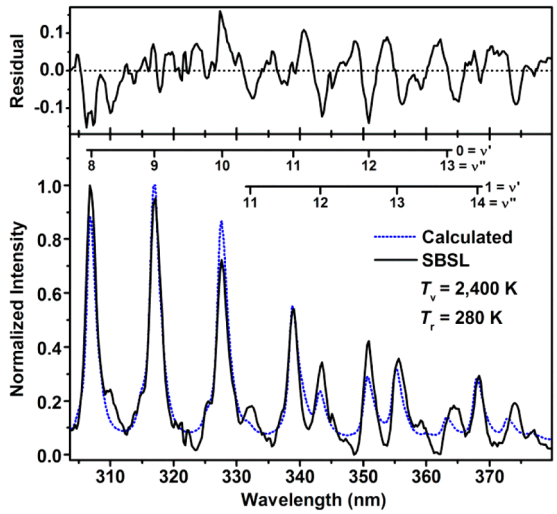

Figure 2. A section of the SBSL spectrum from 80 wt % H_2SO_4 shown in Figure 1 (underlying continuum subtracted) with a least-squares fit simulation of SO emission with T_v = 2400 K and T_r = 280 K. Transitions from the first two vibrational levels of the $B\ ^3\Sigma^-$ excited state ($\nu' = 0$ and 1) to various levels of the $X\ ^3\Sigma^-$ ground state (ν'') are labeled. The upper panel shows the residual (calculated − observed). The root-mean-square deviation is 0.924.

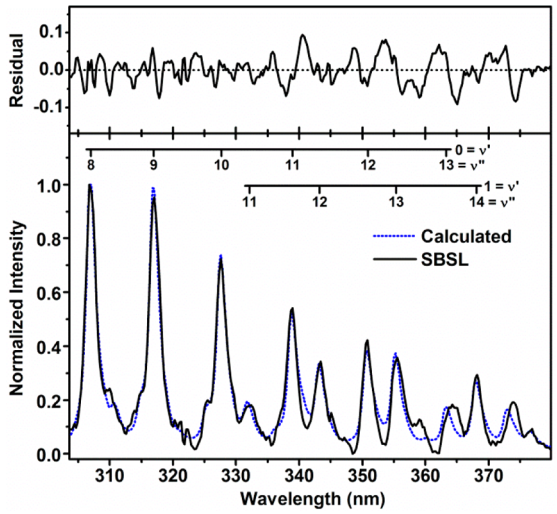

Figure 3. A section of the SBSL spectrum from 80 wt % H_2SO_4 shown in Figure 1 (underlying continuum subtracted) with a least-squares fit simulation of SO emission from a non-Boltzmann vibrational population distribution. Vibrational level populations were floated in the simulation in order to achieve the best-fit spectrum. Transitions from the first two vibrational levels of the $B\ ^3\Sigma^-$ excited state ($\nu' = 0$ and 1) to various levels of the $X\ ^3\Sigma^-$ ground state (ν'') are labeled. The upper panel shows the residual (calculated − observed). Note that the plotted range for the residual is the same as in Figure 2. The root-mean-square deviation is 0.613.

The observation of a non-Boltzmann SO vibrational population distribution has several implications for the events taking place during SBSL. If the SO population is indeed non-Boltzmann in nature, then the observed SBSL emission cannot be described with a single vibrational temperature.[45] Rather, the intracavity conditions are likely varying both spatially and temporally during bubble collapse, thus giving rise to apparent non-equilibrated emission. Indeed, emission may be locally equilibrated in space and time but may have the overall

dx.doi.org/10.1021/jp409222x | J. Phys. Chem. B 2013, 117, 15886−15893

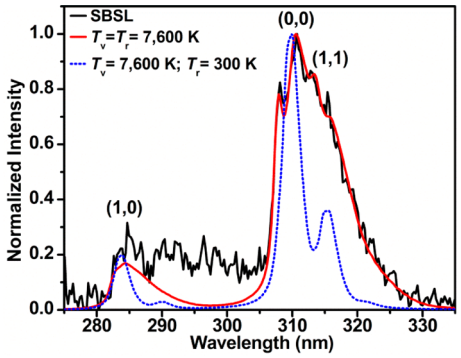

Figure 4. A section of the SBSL spectrum from 65 wt % H_2SO_4 shown in Figure 1 with a least-squares fit simulation of OH emission with T_v = T_r = 7600 K (solid red). A simulated spectrum with T_v = 7600 K and T_r = 300 K (dotted blue) is shown for comparison. Lines resulting from transitions from the first two vibrational levels of the $A\ ^2\Sigma^+$ excited state to the first two levels of the $X\ ^2\Pi$ ground state are labeled.

appearance of non-equilibration in time-averaged measurements. In order to better quantify the precise nature of the events occurring during cavitation, the observed deviation from thermalized emission requires spatiotemporal mapping of the light-emitting region. Recent advances have been made in temporally resolving the SBSL flash from concentrated mineral acid solutions,[46,47] though the signal-to-noise ratio is still insufficient for quantitative analysis of line profiles and intensities. What may be even more challenging is determining the spatial distribution of emitting species during bubble collapse. Further, one needs to determine the relative contribution of temporal and spatial variations to the total observed emission. For example, differences in mass of the emitting species may lead to the formation of shells (think Matryoshka dolls) having distinct conditions with time-averaged spectra being a weighted average of the dynamic contributing regions.[48]

Evidence for the spatial dependence of the observed emission is found by comparing the SO emission temperatures from the 80 wt % solution to those of OH from 65 wt % (Figure 4). First, OH is rotationally hot (≥7600 K), while SO is rotationally cold. Second, T_v for SO is significantly lower (even when considering partial equilibration) than the OH temperatures determined from the 65 wt % solution here (T_v = T_r = 7600 K) despite the 80 wt % solution having a much lower vapor pressure. An even more striking comparison can be made by noting that the OH temperatures from a 65 wt % H_3PO_4 solution were determined to be nearly 10 000 K despite this solution having a vapor pressure nearly 2 orders of magnitude higher than 80 wt % H_2SO_4 (8.7 vs 0.12 Torr, respectively).[9]

The above results indicate that OH emission is occurring from the interior vapor phase of the bubble, while SO emission predominantly takes place within a liquid/vapor shell at the interfacial region. The formation and excitation of SO at the liquid/vapor interface likely occurs via collisions with energetic gas phase neon atoms. Previous work has shown that collisions of neon atoms with H_2SO_4 solution interfaces results in significant energy transfer to the surface molecular species via trapping/desorption.[49−51] The collisions lead to vibrational excitation, heating, and dissociation of interfacial molecular species. Through this process, one may expect the observed T_v of SO to be similar to the translational temperatures of the impacting neon atoms due to high collision rates and rapid equilibration at the interface; the bulk solution acts as a massive heat sink compared to the micrometer-sized cavitation hot spot.

The observation of low T_r for SO and high T_r for OH reflects differences in the formation mechanism, spatial location, and structure of each. The formation and excitation of SO at the liquid/vapor interfacial region may involve a dynamical constraint that results in little torque, and thus low T_r, on the molecule. This could arise from the OH groups being tightly bound in a crystalline-like hydrogen bonding network, thus reducing the tumbling and minimizing recoil of the parent molecules during formation. Indeed, species undergoing trapping/desorption at the liquid/vapor interface are characterized by a Boltzmann translational distribution with cold rotational temperatures,[50] and H_2 molecules leaving a hot silicon surface have also been observed to be rotationally cold due to low torque during formation and desorption.[52] Being in the vapor phase, OH experiences no such dynamical constraint and is free to tumble in any direction upon formation. Further, SO and OH are significantly different in structure due to the relative sizes of the atoms comprising each of the molecules. The rotational cooling rate for the dumbbell-shaped SO is therefore expected to be higher than that for OH with the small hydrogen atom.

To test the hypothesis outlined above, the portion of the SBSL spectrum showing atomic emission was compared to a thermally equilibrated simulation. Figure 5 shows a simulation

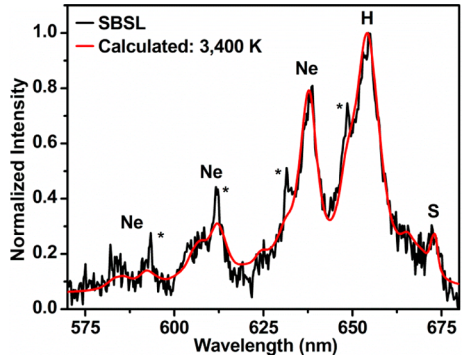

Figure 5. A section of the SBSL spectrum from 80 wt % H_2SO_4 shown in Figure 1 with a least-squares fit simulation (red) of emission from Ne, H, and S atoms, all at T = 3400 K. The spectrum is labeled with the dominant emitter in that region. The Ne lines whose populations are not well-described by a thermally equilibrated Boltzmann distribution are also labeled (*).

of the section of the SBSL spectrum obtained from 80 wt % H_2SO_4 that contains neon, hydrogen, and sulfur atom lines. The least-squares fit simulation indicates a temperature of 3400 K for neon, which matches well with T_v for SO (2400 K). Further, the relative number density of gas phase neon is found to be 9 orders of magnitude higher than that of hydrogen and 13 orders of magnitude higher than that of sulfur, with all at 3400 K. Thus, collision of energetic neon atoms with interfacial species is by far the most statistically probable event. The relatively low temperatures observed for these species may also be indicative of the spatial location from which they are emitting. The interfacial region is likely at a much lower temperature than further within the bubble core due to the proximity to the bulk liquid heat sink. This proximity effect will limit the maximum temperatures achieved. In addition, the opacity of a plasma formed will limit the observable photons to

dx.doi.org/10.1021/jp409222x | J. Phys. Chem. B 2013, 117, 15886−15893

those originating from an outer (cool) transparent shell.[23,47] These effects combine to apply spatial constraints on the observable emission temperatures; emission is observed from an outer, cool shell where neon and SO are essentially thermally equilibrated due to the specific formation and excitation mechanisms at work.

CONCLUSIONS

Analysis of SBSL spectra from H_2SO_4 solutions of different concentration indicates that formation and excitation of the emitting species occurs within distinct spatial locations inside the bubble, and perhaps with additional temporal dependence. Analysis of vibrational and rotational temperatures of molecular species and electronic temperatures of atoms suggests that, for solutions having moderate vapor pressures, the processes leading to SBSL occur predominantly in the vapor phase of the bubble interior. For solutions of low vapor pressure, however, emission is also observed from species that can only originate from the liquid; similar observations in sonochemical reactions have been explained in terms of a two-site model of sonochemical reactivity.[18,39] One mechanism for the excitation of initially liquid phase species is droplet injection into the bubble interior where collisions with energetic gas phase atoms result in pyrolysis of the liquid. A second mechanism is the excitation of liquid phase species formed in hot liquid/vapor shell formed at the interfacial region by collisions of energetic gas phase atoms with molecular species at the liquid-bubble surface. Here, we have shown that, in the absence of droplet injection, emission from excited species that originated in the liquid phase can still be observed. Further, we have found that, for such solutions, assumptions of Boltzmann population distributions are not necessarily valid when considering spatially and temporally averaged emission spectra. These results provide the most detailed picture yet of the intracavity physical and chemical processes occurring during single-bubble cavitation. Further, the observations indicate that the two-site model of sonochemical reactivity[18,39] also applies to single isolated bubbles as well as a cloud of many interacting bubbles.[39,53]

AUTHOR INFORMATION

Corresponding Authors

*E-mail: flan0076@umn.edu. Phone: (612) 625-3867.
*E-mail: ksuslick@illinois.edu. Phone: (217) 333-2794.

Notes

The authors declare no competing financial interest.

ACKNOWLEDGMENTS

This work was supported by NSF (CHE 1011972).

REFERENCES

(1) Crum, L. A.; Roy, R. A. Sonoluminescence. *Science* **1994**, *266*, 233−234.
(2) Putterman, S. J.; Weninger, K. R. Sonoluminescence: How Bubbles Turn Sound into Light. *Annu. Rev. Fluid Mech.* **2000**, *32*, 445−476.
(3) Brenner, M. P.; Hilgenfeldt, S.; Lohse, D. Single-Bubble Sonoluminescence. *Rev. Mod. Phys.* **2002**, *74*, 425−484.
(4) Suslick, K. S.; Flannigan, D. J. Inside a Collapsing Bubble: Sonoluminescence and the Conditions during Cavitation. *Annu. Rev. Phys. Chem.* **2008**, *59*, 659−683.
(5) Hiller, R. A.; Putterman, S. J.; Weninger, K. R. Time-Resolved Spectra of Sonoluminescence. *Phys. Rev. Lett.* **1998**, *80*, 1090−1093.
(6) Didenko, Y. T.; McNamara, W. B., III; Suslick, K. S. Molecular Emission from Single-Bubble Sonoluminescnece. *Nature* **2000**, *407*, 877−879.
(7) Flannigan, D. J.; Suslick, K. S. Plasma Formation and Temperature Measurement during Single-Bubble Cavitation. *Nature* **2005**, *434*, 52−55.
(8) Flannigan, D. J.; Suslick, K. S. Plasma Line Emission during Single-Bubble Cavitation. *Phys. Rev. Lett.* **2005**, *95*, 044301.
(9) Xu, H.; Suslick, K. S. Molecular Emission and Temperature Measurements from Single-Bubble Sonoluminescence. *Phys. Rev. Lett.* **2010**, *104*, 244301.
(10) Storey, B. D.; Szeri, A. J. Water Vapour, Sonoluminescence and Sonochemistry. *Proc. R. Soc. London, Ser. A* **2000**, *456*, 1685−1709.
(11) Toegel, R.; Gompf, B.; Pecha, R.; Lohse, D. Does Water Vapor Prevent Upscaling Sonoluminescence? *Phys. Rev. Lett.* **2000**, *85*, 3165−3168.
(12) Didenko, Y. T.; Suslick, K. S. The Energy Efficiency of Formation of Photons, Radicals, and Ions during Single-Bubble Cavitation. *Nature* **2002**, *418*, 394−397.
(13) Ajello, J. M.; Hansen, D. L.; Beegle, L. W.; Terrell, C. A.; Kanik, I.; James, G. K.; Makarov, O. P. Middle Ultraviolet and Visible Spectrum of SO_2 by Electron Impact. *J. Geophys. Res.: Space Phys.* **2002**, *107*, 1099.
(14) Matula, T. J.; Crum, L. A. Evidence for Gas Exchange in Single-Bubble Sonoluminescence. *Phys. Rev. Lett.* **1998**, *80*, 865−868.
(15) Toegel, R.; Lohse, D. Phase Diagrams for Sonoluminescing Bubbles: A Comparison between Experiment and Theory. *J. Chem. Phys.* **2003**, *118*, 1863−1875.
(16) Flannigan, D. J.; Suslick, K. S. Plasma Quenching by Air during Single-Bubble Sonoluminescence. *J. Phys. Chem. A* **2006**, *110*, 9315−9318.
(17) Gutiérrez, M.; Henglein, A.; Fischer, C. H. Hot-Spot Kinetics of the Sonolysis of Aqueous Solutions. *Int. J. Radiat. Biol.* **1986**, *50*, 313−321.
(18) Suslick, K. S.; Hammerton, D. A.; Cline, R. E. The Sonochemical Hot Spot. *J. Am. Chem. Soc.* **1986**, *108*, 5641−5642.
(19) Kamath, V.; Prosperetti, A.; Egolfopoulos, F. N. A Theoretical Study of Sonoluminescence. *J. Acoust. Soc. Am.* **1993**, *94*, 248−260.
(20) Ashokkumar, M.; Hall, R.; Mulvaney, P.; Grieser, F. Sonoluminescence from Aqueous Alcohol and Surfactant Solutions. *J. Phys. Chem. B* **1997**, *101*, 10845−10850.
(21) Hopkins, S. D.; Putterman, S. J.; Kappus, B. A.; Suslick, K. S.; Camara, C. G. Dynamics of a Sonoluminescing Bubble in Sulfuric Acid. *Phys. Rev. Lett.* **2005**, *95*, 254301.
(22) Flannigan, D. J.; Suslick, K. S. Inertially Confined Plasma in an Imploding Bubble. *Nat. Phys.* **2010**, *6*, 598−601.
(23) Khalid, S.; Kappus, B.; Weninger, K.; Putterman, S. Opacity and Transport Measurements Reveal That Dilute Plasma Models of Sonoluminescence Are Not Valid. *Phys. Rev. Lett.* **2012**, *108*, 104302.
(24) Flannigan, D. J.; Hopkins, S. D.; Camara, C. G.; Putterman, S. J.; Suslick, K. S. Measurement of Pressure and Density Inside a Single Sonoluminescing Bubble. *Phys. Rev. Lett.* **2006**, *96*, 204301.
(25) Flannigan, D. J.; Suslick, K. S. Molecular and Atomic Emission during Single-Bubble Cavitation in Concentrated Sulfuric Acid. *Acoust. Res. Lett. Online* **2005**, *6*, 157−161.
(26) Western, C. M. *PGOPHER, a Program for Simulating Rotational Structure*, 7.0.101; University of Bristol: Bristol, U.K., 2010.
(27) Clerbaux, C.; Colin, R. A Reinvestigation of the $B\ ^3\Sigma^- - X\ ^3\Sigma^-$. *J. Mol. Spectrosc.* **1994**, *165*, 334−348.
(28) Liu, C.-P.; Elliott, N. L.; Western, C. M.; Lee, Y.-P.; Colin, R. The $B\ ^3\Sigma^-$ State of the SO Radical. *J. Mol. Spectrosc.* **2006**, *238*, 213−223.
(29) Yamasaki, K.; Tomita, S.; Hatano, T.; Taketani, F.; Tokue, I. Radiative Lifetime and Multiquantum Vibrational Relaxation of SO ($B\ ^3\Sigma^-$, $\nu' = 3$) by Collisions with He. *Chem. Phys. Lett.* **2005**, *413*, 231−236.
(30) Elks, J. M. F.; Western, C. M. The $A\ ^3\Pi$ State of SO. *J. Chem. Phys.* **1999**, *110*, 7699−7706.

(31) Luque, J.; Crosley, D. R. *LIFBASE: Database and Spectral Simulation Program*, version 2.0.64; SRI International: Menlo Park, CA, 1999.
(32) Eddingsaas, N. C.; Suslick, K. S. Plasma Characteristics of the Discharge Produced during Mechanoluminescence. *Phys. Rev. Lett.* **2007**, *99*, 234301.
(33) Bevington, P. R.; Robinson, D. K. *Data Reduction and Error Analysis for the Physical Sciences*; McGraw-Hill: New York, 2002; pp 146−148.
(34) Ralchenko, Y.; Kramida, A. E.; Reader, J.; NIST ASD Team. *NIST Atomic Spectra Database*, version 3.1.5 [Online]. Available at: http://physics.nist.gov/asd (June 22, 2010); National Institute of Standards and Technology: Gaithersburg, MD.
(35) De Galan, L.; Smith, R.; Winefordner, J. D. Electronic Partition Functions of Atoms and Ions Between 1500 K and 7000 K. *Spectrochim. Acta, Part B* **1968**, *23*, 521−525.
(36) Flannigan, D. J.; Suslick, K. S. Emission from Electronically Excited Metal Atoms during Single-Bubble Sonoluminescence. *Phys. Rev. Lett.* **2007**, *99*, 134301.
(37) Young, T. F.; Maranville, L. F.; Smith, H. M. In *The Structure of Electrolytic Solutions*; Hamer, W. J., Ed.; John Wiley & Sons: New York, 1959; pp 35−63.
(38) Bolsaitis, P.; Elliott, J. F. Thermodynamic Activities and Equilibrium Partial Pressures for Aqueous Sulfuric Acid Solutions. *J. Chem. Eng. Data* **1990**, *35*, 69−85.
(39) Xu, H. X.; Eddingsaas, N. C.; Suslick, K. S. Spatial Separation of Cavitating Bubble Populations: The Nanodroplet Injection Model. *J. Am. Chem. Soc.* **2009**, *131*, 6060−6061.
(40) Fairbrother, D. H.; Johnston, H.; Somorjai, G. Electron Spectroscopy Studies of the Surface Composition in the H_2SO_4/H_2O Binary System. *J. Phys. Chem.* **1996**, *100*, 13696−13700.
(41) Miyamae, T.; Morita, A.; Ouchi, Y. First Acid Dissociation at an Aqueous H_2SO_4 Interface with Sum Frequency Generation Spectroscopy. *Phys. Chem. Chem. Phys.* **2008**, *10*, 2010−2013.
(42) Baldelli, S.; Schnitzer, C.; Shultz, M. J.; Campbell, D. J. Sum Frequency Generation Investigation of Water at the Surface of H_2O/H_2SO_4 Binary Systems. *J. Phys. Chem. B* **1997**, *101*, 10435−10441.
(43) Radüge, C.; Pflumio, V.; Shen, Y. R. Surface Vibrational Spectroscopy of Sulfuric Acid-Water Mixtures at the Liquid-Vapor Interface. *Chem. Phys. Lett.* **1997**, *274*, 140−144.
(44) Flannigan, D. J.; Suslick, K. S. Temperature Nonequilibration during Single-Bubble Sonoluminescence. *J. Phys. Chem. Lett.* **2012**, *3*, 2401−2404.
(45) Ndiaye, A. A.; Pflieger, R.; Siboulet, B.; Molina, J.; Dufreche, J. F.; Nikitenko, S. I. Nonequilibrium Vibrational Excitation of OH Radicals Generated During Multibubble Cavitation in Water. *J. Phys. Chem. A* **2012**, *116*, 4860−4867.
(46) Chen, W. Z.; Huang, W.; Liang, Y.; Gao, X. X.; Cui, W. C. Time-Resolved Spectra of Single-Bubble Sonoluminescence in Sulfuric Acid with a Streak Camera. *Phys. Rev. E* **2008**, *78*, 035301.
(47) Kappus, B.; Khalid, S.; Chakravarty, A.; Putterman, S. Phase Transition to an Opaque Plasma in a Sonoluminescing Bubble. *Phys. Rev. Lett.* **2011**, *106*, 234302.
(48) Bass, A.; Ruuth, S. J.; Camara, C.; Merriman, B.; Putterman, S. Molecular Dynamics of Extreme Mass Segregation in a Rapidly Collapsing Bubble. *Phys. Rev. Lett.* **2008**, *101*, 234301.
(49) Govoni, S. T.; Nathanson, G. M. Exploring the Fate of Water Molecules Striking Concentrated Sulfuric Acid: Scattering Versus Solvation. *J. Am. Chem. Soc.* **1994**, *116*, 779−780.
(50) Nathanson, G. M. Molecular Beam Studies of Gas-Liquid Interfaces. *Annu. Rev. Phys. Chem.* **2004**, *55*, 231−255.
(51) Behr, P.; Scharfenort, U.; Zellner, R. Collisions of Noble Gases with Supercooled Sulfuric Acid-Water Solutions. *Phys. Chem. Chem. Phys.* **2009**, *11*, 7292−7302.
(52) Kolasinski, K. W.; Shane, S. F.; Zare, R. N. Probing the Dynamics of Hydrogen Recombination on Si(100). *J. Chem. Phys.* **1991**, *95*, 5482−5485.
(53) Xu, H.; Glumac, N. G.; Suslick, K. S. Temperature Inhomogeneity during Multibubble Sonoluminescence. *Angew. Chem., Int. Ed.* **2010**, *49*, 1079−1082.